COMPARATIVE EVALUATION OF TEMPERATURE UNIFORMITY INDICES IN FORCED-AIR PRECOOLING OF CHERRIES USING CFD SIMULATION

/

基于 CFD 模拟的樱桃强制空气预冷中温度均匀性指标的比较评估

Binguang JIA*[1, 3], Zhao ZIYU[2], Xiaolong WANG[1, 3], Junting WU[1], Ningning WEI[1], Xiaoming WANG[1]

[1]School of Energy and Machinery, Dezhou University, Dezhou 253023, China

[2] Department of Mechanical and Electrical Engineering, Jinan Engineering Polytechnic, Jinan, 250200 China

[3] Dezhou City Key Laboratory of Energy-saving Technology for Central Air-Conditioning Systems, Dezhou 253023, China

Tel:13688624631.; E-mail: jiabinguang78@163.com

DOI: https://doi.org/10.35633/inmateh-78-74

Keywords: *Temperature uniformity, Forced-air precooling, CFD*

ABSTRACT

Temperature uniformity (σ) during forced-air precooling of fruits and vegetables plays a critical role in preserving quality and extending shelf life. However, inconsistencies in evaluation criteria for calculating σ remain a significant challenge. In this study, cherries were selected as the model system, and computational fluid dynamics (CFD) simulations were employed to analyze three commonly used temperature uniformity indices, namely σ_1, σ_2 and σ_3. The results show that σ_1 is highly sensitive to variations in average temperature during forced-air precooling and becomes unsuitable when the average temperature approaches 0 °C. Moreover, σ_1 yields relatively large values, often exceeding 1. Both σ_2 and σ_3 primarily reflect variations in the temperature range during precooling. However, since σ_2 incorporates temperature in Kelvin in its denominator, its values are generally below 0.1. In contrast, σ_3 remains stable within the range of 0 to 1 throughout the precooling process. Overall, the results indicate that σ_3 is the most suitable index for evaluating temperature uniformity in fruits and vegetables during forced-air precooling.

摘要

果蔬压差预冷过程中的温度均匀性（σ）对于保持其品质和延长其货架期起着至关重要的作用。然而，目前计算 σ 的评价标准不一致。本研究以樱桃为研究对象，利用计算流体动力学（CFD）模拟分析了三种常用的温度均匀性评价方法，即 σ_1、σ_2 和 σ_3。研究结果表明，σ_1 对强制空气预冷过程中平均温度的波动表现出更高的敏感性，并证明在平均温度低于 0℃的条件下无法使用。此外，σ_1 得出的值相对较大，其最大值通常超过 1。σ_2 和 σ_3 主要反映了压差预冷过程中温度范围的变化。然而，由于 σ_2 的分母中包含了开尔文温度，因此所得值通常低于 0.1。相比之下，σ_3 在整个预冷过程中保持 0~1 范围内的稳定值。综合分析表明，σ_3 是评估预冷过程中果蔬温度分布均匀性的最合适指标。

INTRODUCTION

With the rapid development of the economy, the production and sales of fruits and vegetables have shown a year-on-year increasing trend (*Yang et al., 2024*). In 2024, China's vegetable and fruit outputs reached 861.1398 million tons and 339.6581 million tons, respectively (*National Bureau of Statistics of China, 2025*). Limited by the logistics industry in China (*Jia et al., 2026*), which mainly relies on ambient-temperature transportation, the loss rate during the circulation of fruits and vegetables due to traffic conditions and preservation technology is about 30%, which is 4 ~ 5 times that of developed countries in Europe and America, resulting in an annual economic loss of about 100 billion yuan (*Chen et al., 2026*). In order to reduce losses during the circulation of fruits and vegetables, pre-cooling operations are required to quickly remove the field heat after harvest.

Owing to its advantages such as simple operation, wide applicability, low equipment cost, and the ability to utilize existing cold-storage facilities (*Wang et al., 2020*), forced-air precooling has become one of the widely used and effective precooling methods in agricultural product processing, attracting a large number of researchers to study its precooling effectiveness (*Yeboah et al., 2023*) and airflow parameters (*Wang et al., 2026*).

Zhang et al. (2025) analyzed the effects of gradual cooling, delayed cooling, forced-air cooling, and air cooling treatments on the storage quality of kiwifruit. The study found that after 30 days of storage, the firmness of kiwifruit precooled by cooling (GC), delayed cooling (DC), forced-air cooling (FC), and air cooling (AC) was about 20 N, 20 N, 25.1 N, and 34.3 N, respectively, and the soluble solids content showed a similar pattern, indicating that forced-air precooling was an effective method for handling kiwifruit. *Tao et al. (2024)* systematically compared multiple pre-cooling techniques. The results showed that, compared with vacuum pre-cooling and hydrocooling, forced-air precooling not only completed pre-cooling efficiently within 20 minutes but also performed most prominently in delaying fruit softening and senescence, maintaining firmness, acidity, and nutritional qualities such as vitamin C. *Yeboa et al. (2023)* investigated the synergistic preservation effect of forced-air precooling and modified atmosphere packaging, finding that the combination of "forced-air precooling + modified atmosphere packaging" most effectively delayed fruit ripening and quality deterioration, significantly reduced weight loss, maintained firmness and color, and better preserved soluble sugars and antioxidant substances. *Mahajan et al. (2023)* compared the effects of forced-air cooling, hydrocooling, and evaporative precooling on the storage quality of pears, and found that forced-air cooling could most effectively maintain the postharvest quality of the fruit, successfully extending the ambient-temperature shelf life of pears from 10 days to 15 days. *Shilpa Mahajan et al. (2022)* evaluated the effects of different durations of forced-air cooling treatments on the preservation of litchi and indicated that a 6 hours forced-air precooling treatment most effectively inhibited weight loss and enzymatic browning, while better maintaining peel color, firmness, sugar-acid components, and active substance contents such as anthocyanins and total phenolics, significantly extending the storage life of litchi by up to 14 days.

Increasing the airflow velocity can significantly reduce precooling time, but relevant studies point out that the relationship between air velocity and precooling time is non-linear. *Liu et al. (2021)* established a mathematical model for forced-air precooling of cherries using the finite volume method, and finding that the 7/8 pre-cooling time decreased with increasing air velocity, but when the air velocity exceeded 2 m/s, the 7/8 precooling time did not shorten significantly. However, excessively high airflow velocities lead to higher energy consumption and moisture loss in fruits and vegetables (*Jia et al., 2022*). Based on the influence of airflow velocity on pressure drop and precooling time, it can be concluded that there exists an optimal airflow velocity in forced-air cooling that rapidly reduces the temperature of produce while maintaining low precooling energy consumption (*Wang et al., 2022*). *Han et al. (2017)* and *Hussain et al. (2021)* taking single apples and citrus fruits as research objects, respectively, obtained optimal airflow velocities of 0.4 ~ 1.0 m/s and 2.0 m/s.

Due to the different sequence of contact with the cold air during pre-cooling process, the temperature difference between the windward and leeward sides of fruits and vegetables varies, resulting in a temperature gradient along the airflow direction inside the produce (*Zhang et al., 2024*). To ensure that all fruits and vegetables reach the target pre-cooling temperature, the cooling time must be increased, but this may also cause chilling injury on the windward side due to excessively low temperatures (*Zuo et al., 2025*). Therefore, studying the cooling characteristics of fruits and vegetables during pre-cooling and improving the temperature distribution uniformity both during and at the end of precooling is of great significance. *Xie et al. (2019)* comprehensively analyzed the factors affecting the uniformity of forced-air precooling of apples, finding that the four factors influencing uniformity, in descending order of impact, were: supply air temperature, airflow velocity, vent size, and vent arrangement. *Jin et al. (2021)* established a mathematical model for forced-air precooling of apples. Through numerical simulation, they found that adopting a vertical airflow mode could reduce the 7/8 cooling time and non-uniformity by 17% and 40%, respectively. *Kumar et al. (2023)* taking apples as the research object, analyzed the effect of alternating airflow modes on temperature uniformity. They discovered that at an airflow velocity of 3 m/s, alternating the airflow direction three times could reduce the non-uniformity of apples by 43.89%.

Although numerous studies have investigated temperature non-uniformity during forced-air precooling of fruits and vegetables, the uniformity calculation methods used by the aforementioned scholars are inconsistent, resulting in significant differences in the obtained non-uniformity values. Therefore, selecting a widely applicable and conveniently expressed uniformity calculation method is crucial for understanding precooling uniformity. Based on computational fluid dynamics (CFD), this paper uses cherries as the material to calculate the temperature distribution inside the precooling packaging box, analyzes the applicability of several commonly used precooling uniformity calculation methods, aiming to identify the most suitable method for calculating precooling uniformity.

MATERIALS AND METHODS

Physical model and mesh generation

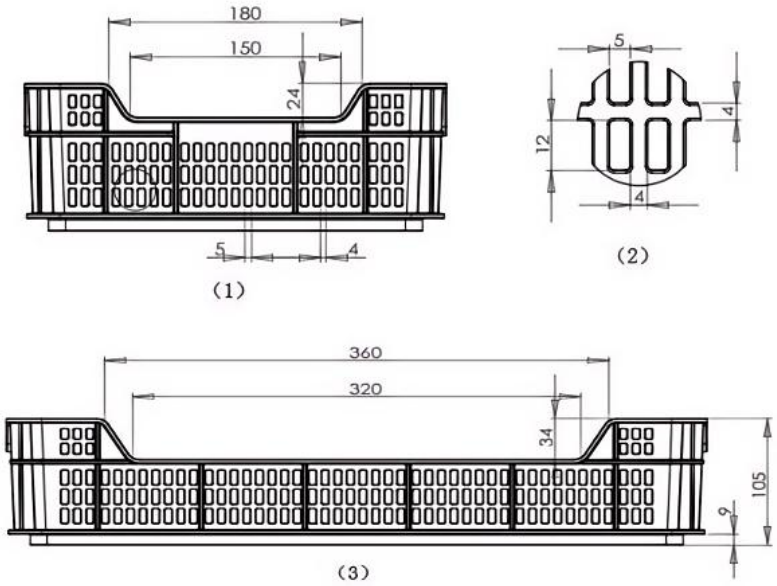

Fig. 1 - Geometric structure of packages

Using Gambit software, a physical model of the packaging box and the cherries contained within it was developed. The dimensions of the commonly used commercial packaging box are 470 mm × 270 mm × 94 mm. The central opening is trapezoidal, with an upper base of 360 mm, a lower base of 320 mm, and a height of 34 mm. Both the windward and leeward sides are perforated with rectangular holes of 12 mm × 4 mm, with a spacing of 4 mm between adjacent holes. The detailed structure is shown in Fig. 1. A cherry is more accurately approximated as an oblate spheroid with a central indentation rather than a perfect sphere. To quantify its physical dimensions, a simplified geometric model based on a triaxial ellipsoid was adopted. This model defines three mutually perpendicular principal axes, corresponding to the transverse, longitudinal, and vertical diameters. These dimensions were measured using a vernier caliper. According to Jia et al. (2020), the transverse, longitudinal, and vertical diameters of the cherry are 26.47 mm, 22.11 mm, and 22.05 mm, respectively. Furthermore, to minimize the influence of air recirculation on the numerical simulation results, the computational domain downstream of the packaging box was extended by 500 mm (Cao et al., 2020). The established physical model for forced-air precooling of cherries is shown in Fig. 2.

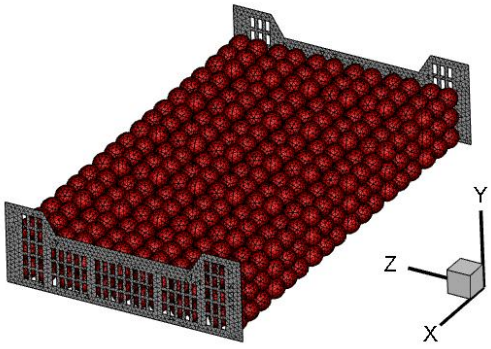

Fig. 2 - Physical model

Gambit was utilized to mesh the physical model. As shown in **Fig. 3**, the hexahedral/wedge (Hex/Wedge) mesh in the air channel region was generated using the Cooper scheme, while the tetrahedral/hybrid (Tet/Hybrid) mesh for the interior space of the cherries and the packages was generated using the TGrid scheme. To ensure convergence of the numerical simulation and maintain mesh quality at the contact points between fruits and between fruits and walls of the package, a small gap was left between walls of packages and the fruits, as well as between the fruits themselves.

To improve the accuracy and computational speed of the model, a grid independence study was necessary. **Table 1** presents the 7/8 precooling times of cherries when the total mesh counts were 5.6×10⁶, 9.2×10⁶, 10.8×10⁶, 13.2×10⁶, and 16.2×10⁶, respectively. As shown in Table 1, when the total mesh count reached 13.2×10⁶, the variation in results became negligible. Therefore, considering both computational accuracy and speed, a mesh count of 13.2×10⁶ was adopted.

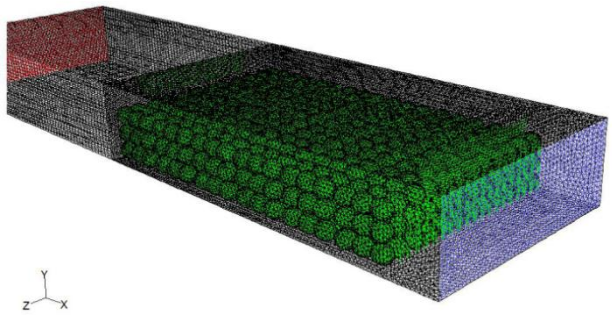

Fig. 3 - Meshing of the physical model

Table 1

Pre-cooling time for different mesh numbers

Mesh numbers	5.6×10⁶	9.2×10⁶	10.8×10⁶	13.2×106	16.2×10⁶
Pre-cooling time / min	Diverge	41.6	40.8	40.5	40.4

Assumption and simulation settings

For the convenience of mathematical model establishment and calculation, necessary assumptions were made for the precooling process: (1) The precooling process was a three-dimensional unsteady heat transfer (*Han et al., 2015*); (2) Air was an incompressible fluid (*Jia, 2019*); (3) Contact between individual items and radiation heat transfer are neglected (*Wang et al., 2023*); (4) The influence of buoyancy on the cold air during flow was neglected (*Jia, 2019*); (5) Water evaporation and viscous dissipation of air are neglected **Error! Reference source not found.***Chen et al., 2024*).

The finite volume method was used to discretize the governing equations (including the continuity, momentum, and energy equations) (*Han et al., 2023*). The SIMPLE algorithm was employed for pressure-velocity coupling. The PRESTO! scheme was applied for spatial discretization of pressure, while the second-order upwind scheme was adopted for discretizing the momentum, turbulent kinetic energy, turbulent dissipation rate, and energy equations to enhance computational accuracy (*Yang et al., 2024*).

Governing equations of air zones

For the flow and heat transfer in the air domain, which involved unsteady, incompressible fluid, the governing equations based on the mean Reynolds-averaged approach, as given in:

$$\frac{\partial \rho_a}{\partial t}+\frac{\partial\left(\rho_a u_i\right)}{\partial x_i} \tag{1}$$

$$\frac{\partial}{\partial t}\left(\rho_a u_i\right)+\frac{\partial}{\partial x_j}\left(\rho_a u_i u_j\right)=-\frac{\partial P}{\partial x_i}+\frac{\partial}{\partial x_j}\left[\mu_a\left(\frac{\partial u_i}{\partial x_j}+\frac{\partial u_j}{\partial x_i}\right)\right]-\frac{\partial}{\partial x_j}\left(\rho_a \overline{u_i' u_j'}\right)-\rho_a g \tag{2}$$

$$\frac{\partial}{\partial t}(\rho_{\alpha} c_{p,a} T)+\frac{\partial}{\partial x_j}(\rho_a c_{p,a} u_j T)=\frac{\partial}{\partial x_j}(\lambda_{\alpha}\frac{\partial T}{\partial x_j})-\frac{\partial}{\partial x_j}(\rho_{\alpha} c_{p,a}\overline{u_j' T'}) \tag{3}$$

where: t is time, [s]; P - pressure, [Pa]; u_i - the air velocity, [m/s]; x_i - Cartesian coordinates, [m]; ρ_a - air density, [kg/m³]; μ_a - dynamic viscosity of air, [Pa·s]; $\rho_a\overline{u_i' u_j'}$ - Reynolds stress tensor component, [Pa]; u_i' - the fluctuating velocity of air, [m/s]; g - gravitational acceleration, [m/s²]; λ_a - thermal conductivity of air, [W/(m·K)]; T' - the fluctuating temperature of air, [K].

According to the calculation method for the Reynolds number (*Huang et al., 2025*), when the air supply velocity ranged from 0.5 m/s to 3.0 m/s, the Reynolds number reaches 4700 ~ 28,000. Therefore, the air flow during forced-air precooling of cherries was turbulent. The standard k-ε equations were shown in Eqs. (4) and (5).

$$\frac{\partial(\rho_a k)}{\partial t}+\nabla\cdot(\rho_a\vec{u}k)=\nabla\cdot\left[\left(\mu_a+\frac{\mu_t}{\sigma_k}\right)\nabla k\right]+P_k-\rho\varepsilon \quad (4)$$

$$\frac{\partial(\rho_a \varepsilon)}{\partial t}+\nabla\cdot(\rho_a\vec{u}\varepsilon)=\nabla\cdot\left[\left(\mu_a+\frac{\mu_t}{\varepsilon_k}\right)\nabla\varepsilon\right]+C_{1\varepsilon}\frac{\varepsilon}{k}P_k-C_{2\varepsilon}\rho_a\frac{\varepsilon^2}{k} \quad (5)$$

In Eqs. (4) and (5), the turbulent viscosity (μ_t) is given by:

$$\mu_t=\rho_a C_\mu\frac{k^2}{\varepsilon} \quad (6)$$

where: k is turbulent kinetic energy, [m²/s²]; ε - turbulent dissipation rate, [m²/s³]; μ_t - turbulent eddy viscosity, [Pa·s]; $\vec{u}$ - velocity vector, [m/s]; σ_k- turbulent Prandtl number for k [dimensionless]; P_k - production term of turbulent kinetic energy, [kg/(m·s³)]; $C_{1\varepsilon}$,$C_{2\varepsilon}$ and C_μ - constant number, [dimensionless].

Governing equations of cherries

The main internal heat source in cherries was their own respiratory heat, which was applied as an internal heat source to the heat conduction differential equation in the cherry region. The governing equation was as follows (*Wang et al., 2019*):

$$\rho_c c_{p,c}\frac{\partial T_c}{\partial t}=\lambda_c\nabla^2 T_c+S_e \quad (8)$$

$$S_e=\frac{Q_r}{V} \quad (9)$$

where: ρ_c is the density of cherries, [kg/m³]; $c_{p,c}$ - the specific heat capacity of cherries, [J/ (kg·K)]; λ_c - the thermal conductivity of cherries, [W/(m·K)]; T_c - the temperature of cherries, [K]; S_e - the internal heat source of cherries, [W/m³]; Q_r - the respiratory heat of cherries, [W]; V - the volume of cherries, [m³].

According to the law of conservation of energy, the heat released by cherries per unit volume should equal the heat absorbed by air per unit volume. Considering the shape of the physical model mentioned above, the thermal balance equation at the fluid-solid coupling interface between cherries and air was given as follows (*Han et al., 2023*):

$$(\lambda_a\nabla T_a-\lambda_c\nabla T_c)n_{ac}=-h_{a-c}(T_c-T_a) \quad (10)$$

where: n_{ac} is the unit normal vector perpendicular to the cherry-air interface [dimensionless]; h_{a-c} is the convective heat transfer coefficient at the cherry surface, [W/(m²·K)].

Boundary conditions and material properties

Among them, the thermal physical parameters of the fruits and vegetables that vary with temperature are calculated, with a summary of the physical parameters provided in Table 2. For the forced-air pre-cooling outer packaging box, a velocity inlet boundary condition was applied at the inlet, and a pressure outlet was set at the cold air exit. The outer walls of the packaging box were treated as no-slip walls. The initial temperature for both cherries and the air inside the model was set to 26°C.

Table 2

Summary of physical parameters (*Jia, 2019*)

Name	Density/ (kg·m⁻³)	Specific heat capacity/ J / (kg·K)	Thermal conductivity / W/(m·K)
Cherry	1061.93	$c_{p,c}=-5.45\times10^{-3}T^2-1.54T+3187.5$	$\lambda_c=-1.62\times10^{-5}T^2+1.08T-1.62\times10^{-5}$
Packages	942	2250	0.21
Air	1.225	1006.43	0.0242

Temperature non-uniformity

Currently, research on the non-uniformity during precooling of fruits and vegetables mainly adopts two approaches:

(1) Select several temperature measurement points within the precooled produce, and use the standard deviation in mathematical statistics, which reflects the degree of data dispersion, to represent the temperature non-uniformity during precooling (*Kumar et al., 2023*). Depending on the temperature scale used (Celsius or

Kelvin), it was denoted Eqs. (11) and (12), respectively. This method was also frequently employed in studies on the non-uniform distribution in refrigeration and cryogenic equipment, such as in liquid distributors and header designs of heat exchangers (*Lee, 2010*).

$$\sigma_1 = \frac{n}{\sum_{i=1}^{n} T_i} \sqrt{\frac{1}{n-1} \sum_{i=1}^{n} (T_i - \frac{1}{n} \sum_{i=1}^{n} T_i)^2} \tag{11}$$

$$\sigma_2 = \frac{n}{\sum_{i=1}^{n} T_{i,K}} \sqrt{\frac{1}{n-1} \sum_{i=1}^{n} (T_{i,K} - \frac{1}{n} \sum_{i=1}^{n} T_{i,K})^2} \tag{12}$$

where: σ_1 is temperature non-uniformity [dimensionless]; n - number of temperature measurement points [dimensionless]; T_i - the temperature measured at the i-th point, [°C]; σ_2 - standard deviation representing temperature non-uniformity in K scale [dimensionless].

(2) Additionally, the degree of dispersion of the dimensionless temperature parameter (Y) at measurement points could be used to reflect the uniformity of temperature distribution (*Olatunji et al., 2017*). Here, Y represented the proportion of agricultural products that have not yet reached the target cooling temperature relative to the entire batch, shown in Eq. (13), leading to the calculation method for temperature non-uniformity (Eq. (14)) (*Gruyters et al., 2020*):

$$Y_i = (T_i - T_a)/(T_s - T_a) \tag{13}$$

$$\sigma_3 = \max\{Y_i - \frac{1}{n} \sum_{i=1}^{n} Y_i\} - \min\{Y_i - \frac{1}{n} \sum_{i=1}^{n} Y_i\} \tag{14}$$

where: Y_i is dimensionless temperature parameter at measurement point i, [dimensionless].

RESULTS AND DISCUSSION

Verification

To validate the model, the measured and predicted temperatures were compared based on the Root Mean Square Error (RMSE) and Mean Absolute Percentage Error (MAPE) (see Eqs. (15) and (16)) (*Chen et al., 2024*).

$$RMSE = \sqrt{\frac{1}{n} \sum_{n=1}^{n} (E_i - S_i)^2} \tag{15}$$

$$MAPE = \frac{1}{n} \sum_{i=1}^{n} \frac{|E_i - S_i|}{E_i} \times 100\% \tag{16}$$

where: E_i is the experimental or actual observed value for the i-th data point; S_i - the simulated or predicted value corresponding to the i-th data point.

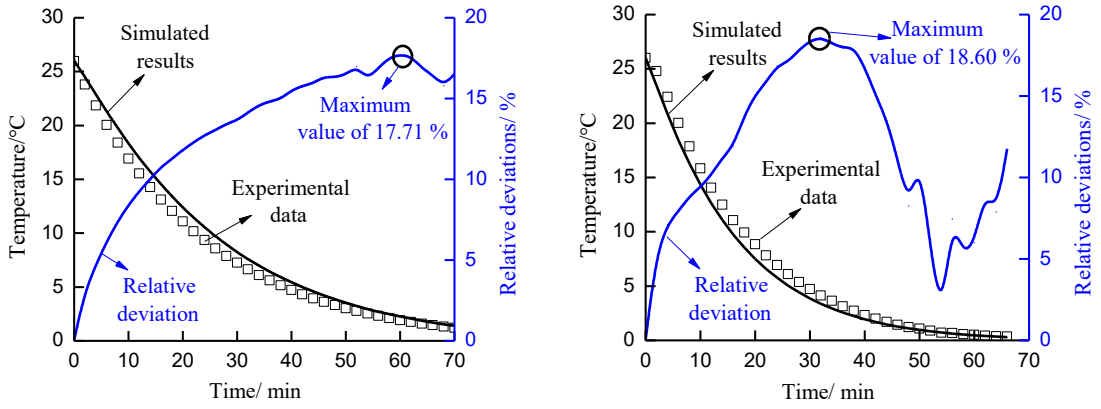

Fig. 4 - Comparison of experimental data and simulation results
a) Air velocity of 0.72 m/s; b) Air velocity of 1.45 m/s

Fig. 4 shows a comparison between the simulated cooling curves and the experimental values reported in reference (*Jia, 2019*) for forced-air precooling of cherries at air velocities of 0.72 m/s and 1.45 m/s.

As shown in Fig. 4, good agreement is observed between the experimental and simulated temperature curves at both air velocities. The maximum values of RMSE and MAPE for the two cases are 1.44 °C and 1.60 °C, and 17.71% and 18.60%, respectively. The discrepancies between the experimental and simulation results can be attributed to the following factors: (1) In the experiments, the cherries were randomly stacked within the packages, leading to variability in airflow distribution. (2) When temperature sensors such as thermocouples are used, the measurement locations may not exactly coincide with the corresponding nodes in the simulation grid, resulting in some dispersion in the experimental data. Overall, the comparison between experimental and simulation results indicates that the established mathematical model can reliably predict the temperature distribution during forced-air precooling of cherries.

Comparison of three types of temperature non-uniformity

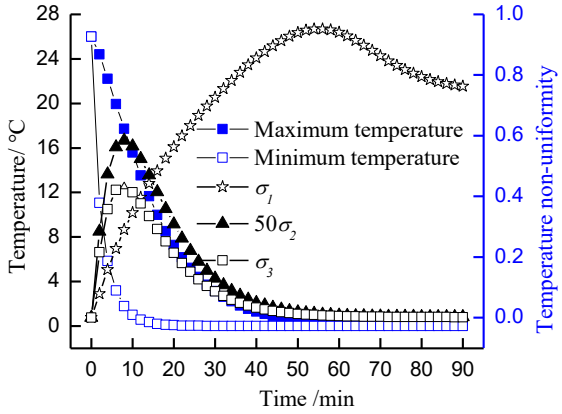

Fig. 5 - Relationship between temperature non-uniformity and temperature

Fig. 5 illustrates the relationship between the temperature non-uniformity and temperature. As shown in Fig. 5, during the forced-air precooling process, the temperature of the cherries gradually decreases, while the temperature non-uniformity indices (σ_1, $50\sigma_2$, and σ_3) initially increase and then decrease. The use of $50\sigma_2$ instead of σ_2 is due to the relatively small magnitude of σ_2, which is not suitable for clear graphical representation. However, the trends of σ_1, $50\sigma_2$, and σ_3 exhibit noticeable differences. Specifically, σ_1 reached its maximum value between 50 and 60 minutes, whereas $50\sigma_2$ and σ_3 peaked at approximately 10 minutes. Analysis of the relationship between the temperature non-uniformity indices (σ_1, $50\sigma_2$ and σ_3) and the maximum and minimum temperature profiles indicates that the peak of σ_1 occurred in the later stage of forced-air precooling (50 ~ 60 min), when the maximum and minimum temperatures of the cherries converged. In contrast, the peaks of $50\sigma_2$ and σ_3 appeared near the time of the maximum temperature difference (around 10 min), after which their values decreased rapidly and approached zero by 50 ~ 60 min. The trends of $50\sigma_2$ and σ_3 were consistent, differing only in magnitude.

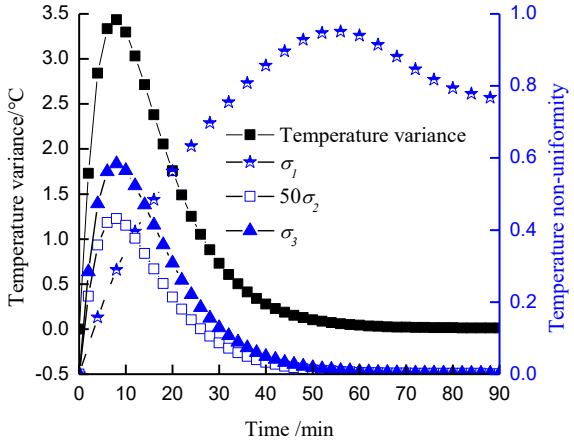

Fig. 6 - Profiles of temperature non-uniformity and temperature variance over time

As shown in Fig. 6, the three temperature non-uniformity indices (σ_1, $50\sigma_2$, and σ_3) reflect temperature changes during the forced-air precooling process to different extents. To further clarify the relationship between these indices and temperature variation, Fig. 6 illustrates the influence of temperature variance on the non-uniformity indices. The results indicate that the temporal variations of $50\sigma_2$ and σ_3 are fully consistent with that of temperature variance, with their extreme values occurring at the maximum temperature variance. In contrast, σ_1 exhibits an opposite trend, with its extreme value appearing near the minimum temperature variance.

Figure 7 illustrates the relationship between the three temperature non-uniformity indices (σ_1, $50\sigma_2$, and σ_3) and the average temperature. As the temperature decreases and before the average temperature approaches 0 °C, the value of σ_1 increases, with its rate of increase becoming more pronounced as the temperature decreases, reaching a peak near 0 °C. The trends of $50\sigma_2$ and σ_3 are similar: both initially increase and then decrease with decreasing temperature, with peak values occurring in the intermediate cooling range (10 ~ 12 °C). Based on the above analysis, σ_1 differs significantly from $50\sigma_2$ and σ_3. This difference can be explained by examining Eqs. (11) ~ 14). In the calculation of σ_1, $50\sigma_2$, and σ_3, the use of different temperature units (°C and K) results in different denominators, leading to distinct sensitivities to the average temperature. Specifically, the denominator of σ_1 ranges from 26 °C to 0 °C, whereas that of $50\sigma_2$ ranges from 273 K to 299 K. Therefore, under the same temperature variance, the average temperature affects the non-uniformity indices differently. Figure 7 further illustrates the variation of σ_1 and $50\sigma_2$ with average temperature per unit temperature variance. As the average temperature decreases, σ_1 increases and rises sharply when the temperature falls below 9 °C. As the average temperature approaches 0 °C, σ_1 tends toward infinity. If the forced-air precooling temperature is below 0 °C, the average temperature may reach or fall below 0 °C, causing σ_1, as calculated from Eq. (11), to approach infinity. This behavior may complicate the analysis of the effect of air temperature on the cooling process. In contrast, the variation of $50\sigma_2$ with average temperature is relatively smooth, with an approximately constant rate of change. According to Eqs. (13) ~ (14), σ_3 is derived from the difference between extreme values after temperature nondimensionalization. Therefore, similar to $50\sigma_2$, it primarily reflects the temperature range (i.e., the difference between maximum and minimum temperatures).

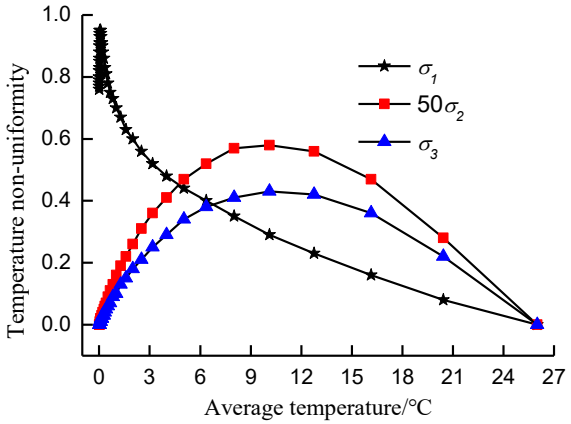

Fig. 7 - Variation of temperature non-uniformity with average temperature

CONCLUSION

This study evaluates three commonly used methods for assessing precooling non-uniformity, based on previous research, through CFD modeling. The results indicate that σ_1, σ_2, and σ_3 can all reflect the temperature distribution during forced-air precooling. However, the analysis reveals that these indices differ in their sensitivity and physical interpretation. Specifically, σ_1 is more sensitive to the influence of average temperature, reflecting the proportional relationship between the temperature range and the mean temperature, whereas σ_2 and σ_3 primarily characterize variations in the temperature range.

Furthermore, σ_1 may encounter computational instability when the average temperature approaches 0 °C, as its denominator tends toward zero, limiting its applicability to temperatures above 0 °C. The numerical values of σ_2 are relatively small (with extreme values during precooling typically less than 0.1), which reduces its practical convenience for non-uniformity evaluation.

In contrast, σ_3 combines the advantages of the other two indices: it is applicable across the full temperature range, and its values lie between 0 and 1, facilitating interpretation and application. Therefore, σ_3 is identified as the most suitable index for evaluating temperature non-uniformity during forced-air precooling.

ACKNOWLEDGEMENT

This work was supported by the Doctoral Fund of Dezhou University (NO. 4022504135).

REFERENCES

[1] Cao Y., Gong Y. F., Zhang X. R., (2020), Impact of ventilation design on the precooling effectiveness of horticultural produce-a review, Food Quality and Safety, 4(1), pp.29-40.

[2] Chen Q., Qian J., Yang H., Li J., Lin X., Wang B. (2024), Multiscale coupling analysis and modeling of airflow and heat transfer for warehouse-packaging-kiwifruit under forced-air cooling, *Biosystems Engineering*, vol. 244, pp.166-176.

[3] Chen X., Wang Y., Sheng W., Zheng H., Bayizi M., Pan S., Liu S., Li D. (2025), Influence of Opening Size and Position on the Performance of Forced-Air Precooling of Apples, *Journal of Food Process Engineering*, vol. 48, no.1, e70024.

[4] Chen Y., Zhao M., Linghu B., Song H., (2026), Differential pressure pre-cooling of layered peaches: Airflow distribution and cooling effectiveness in relation to the stacking pattern by using CFD, *Postharvest Biology and Technology*, vol. 234, 114071.

[5] Gruyters W., Van De Looverbosch T., Wang Z., Janssen S., Verboven P., Defraeye T., Nicolaï B. M. (2020), Revealing shape variability and cultivar effects on cooling of packaged fruit by combining CT-imaging with explicit CFD modelling, *Postharvest Biology and Technology*, vol. 162, 111098.

[6] Han J. W., Badía-Melis R., Yang X. T., Ruiz-Garcia L., Qian J. P., Zhao C. J. (2017), CFD simulation of airflow and heat transfer during forced-air precooling of apples, *Journal of Food Process Engineering*, vol. 40, no.2, e12390.

[7] Han J. W., Ren Q. S., Li J. C., Zhu W. Y., Yang, X. T. (2023), Numerical analysis of coupled heat and mass transfer processes in packaged tomatoes throughout the cold chain, *Case Studies in Thermal Engineering*, vol. 42, 102687.

[8] Han J. W., Zhao C. J., Yang X. T., Qian J. P., Fan B. L. (2015), Computational modeling of airflow and heat transfer in a vented box during cooling: Optimal package design, *Applied Thermal Engineering*, vol. 91, pp.883-893.

[9] Huang K. M., Guan Z., Hammami A. (2022), The US fresh fruit and vegetable industry: an overview of production and trade, *Agriculture*, vol. 12, no. 10, 1719.

[10] Huang X., Wang L., Li X., (2025), Research on thermal performance and pressure loss of a new perforated-folded baffle solar air collector, *Numerical Heat Transfer, Part A: Applications*, vol. 86, no. 4, pp.976-995.

[11] Hussain T., Kamal M. A., Hafiz A., (2021), Comparative analysis of apple and orange during forced convection cooling: experimental and numerical investigation, *AIMS Energy*, vol. 9, no. 2, pp.193-212.

[12] Jia B., Liu F., Yuan S., Li Z., Zhang X. (2021), The effect of alternating ventilation on forced air pre-cooling of cherries, *International Journal of Food Engineering*, vol. 17, no. 6, pp.423-433.

[13] Jia B., Wang X., Hou Q., Hu M., Zhang Q., Sun G., Xin Y. (2026), Parametric analysis and optimal air velocity selection in forced air pre-cooling: effects of packaging quantity, *International Journal of Food Engineering*, (Ahead of Publication).

[14] Jia B., Yang L., Zhang L., Li X., Liu B., Chen F., Zhang Q. (2022), Energy consumption in relation to the number of stacked packages in forced air pre-cooling of apples, *Journal of Food Process Engineering*, vol. 45, no. 5, e14021.

[15] Jin T., Li B., Zhu Z., Han S., Wei J., (2021), Simulation and Analysis of Forced-air precooling of Apples with Vertical Air Supply (苹果垂直送风式压差预冷性能模拟与分析), *Transactions of the Chinese Society for Agricultural Machinery*, 52(9), Hangzhou, China, ISSN:1000-1298, pp.369-375,

[16] Kumar A., Kumar R., Subudhi S., (2023a), Experimental investigations of periodic airflow reversal during forced-air cooling of Apples: Impacts on cooling rate and uniformity, *Journal of Food Engineering*, vol. 359, 111684.

[17] Kumar A., Kumar R., Subudhi S., (2023b), Numerical modeling of forced-air pre-cooling of fruits and vegetables: A review, *International Journal of Refrigeration*, vol. 145, pp.217-232.

[18] Lee J. K., (2010), Optimum channel intrusion depth for uniform flow distribution at header-channel junctions, *Journal of Mechanical Science and Technology*, vol. 24, no. 7, pp.1411-1416.
[19] Liu F., Jia B., Li Z., Zhang X. (2021), Thermodynamics analysis for forced air pre-cooling of cherry, *Journal of Food Process Engineering*, vol. 44, no.11, e13881.
[20] Mahajan K., Gupta S. K., Sharma S. R., Singh N. P., Kanojia V. (2023), Evaluation of precooling methods for shelf-life enhancement of pear (Pyrus spp.) fruits under ambient storage, *The Indian Journal of Agricultural Science*s, vol. 93, no.1, pp.116-118.
[21] Olatunji J. R., Love R. J., Shim Y. M., Ferrua M. J., East A. R. (2017), Quantifying and visualising variation in batch operations: a new heterogeneity index, *Journal of Food Engineering*, 196, pp.81-93.
[22] Shilpa Mahajan B. V. C., Singh N. P., Bhullar K. S., Kaur S. (2022), Forced air cooling delays pericarp browning and maintains post-harvest quality of litchi fruit during cold storage, *Acta Physiologiae Plantarum*, vol. 44, no. 6, pp. 66.
[23] Sui S., Wang Y., Ma J., Sun L., Huang G., Li J. (2022). Modeling and Simulation of Temperature Fields in the Process of Pressure-Difference Precooling of Loquats in Multiple Rows of Cartons, *Proceedings of the 2022 2nd International Conference on Bioinformatics and Intelligent Computing*, Harbin/ China, pp. 475-483.
[24] Tao S., Wang J., Xie J., (2024), Influence of different pre-cooling methods on the postharvest storage of 'Kyoho'grapes (Vitis labrusca× vinifera 'Kyoho'), *Food Quality and Safety*, vol. 8, fyae033.
[25] Wang D., Lai Y., Jia B., Chen R., Hui X. (2020), The optimal design and energy consumption analysis of forced air pre-cooling packaging system, *Applied Thermal Engineering*, vol. 165, 114592.
[26] Wang D., Lai Y., Zhao H., Jia B., Wang Q., Yang X. (2019), Numerical and experimental investigation on forced-air cooling of commercial packaged strawberries, *International Journal of Food Engineering*, vol. 15, no.7, 20180384.
[27] Wang G. B., Wang Y. Z., Zhang X. R., (2023), Non-linear heat and mass transfer in packed spherical horticultural produce: Heterogeneity and irreversibility, *International Communications in Heat and Mass Transfer*, vol. 146, 106910.
[28] Wang X. F., Fan Z. Y., Li B. G., Liu S., (2022), Forced-air cooling of iceberg lettuces: Cooling efficiency in relation to commercial operating strategies, *International Journal of Refrigeration*, vol. 139, pp. 84-92.
[29] Wang Y., Ma J., Liu J., (2025), Effects of Different Precooling Methods on the Storage and Preservation Quality of Summiton Sweet Cherry (不同预冷方式对萨米脱甜樱桃贮藏保鲜品质的影响), *Journal of Fruit Resources*, vol. 6, no.6, Tianshui, China, ISSN:2096-8108 pp.22-26.
[30] Xie H., Zhang J., Zhang., Deng S., (2019), Experimental Research on Uniformity of Differential Pressure Precooling of Apple (苹果差压预冷均匀性的实验研究), *Food Research and Development*, vol. 40, no. 5, Jinan, China, ISSN: 1005-6521, pp.42-47.
[31] Yang G., Zhang Q., (2024), Analysis of the Development Status and Marketing Strategies of China's Fresh Agricultural Products Industry (我国生鲜农产品行业发展现状及营销对策浅析), *South China Agriculture*, vol. 18, no. 9, ISSN: 1673-890X, pp.196-200.
[32] Yang L., Jia B., Zhang Q., Zou Z. (2024), Effect of dynamic contact angle behavior on droplet topological structure and film thickness evolutions in droplet mode, *Desalination*, vol. 576, 117359.
[33] Yeboah S., Hong S. J., Park Y., Choi J. H., Eum H. L. (2023), Postharvest quality improvement of bell pepper (Capsicum annuum L. CV Nagano) with forced-air precooling and modified atmosphere packaging, *Foods*, vol. 12, no. 21, 3961.
[34] Zhang J., Teng J., Liang J., Gibson B. W., Zhang W., Li A., Cheng Y., Zeng Y. (2025), Effect of different pre-cooling strategies on the storage quality of kiwifruit, *Scientia Horticulturae*, vol. 344, 114105.
[35] Zhang J., Zhang W., Liang J., He B., Ding G., Cheng Y., Deng X., Zeng Y. (2024), A physical twin model for simulation of kiwifruit core temperature during pre-cooling and cold storage, *Postharvest Biology and Technology*, vol. 212, 112862.
[36] Zhao H., Liu S., Tian C., Yan G., Wang D. (2018), An overview of current status of cold chain in China, *International Journal of Refrigeration*, vol. 88, pp.483-495.
[37] Zuo X., Wang J., Wu Z., Jin P., Zheng Y. (2025), High relative humidity storage mitigates chilling injury in zucchini fruit via regulating the CpMYB63-mediated cell wall degradation, *Postharvest Biology and Technology*, vol. 222, 113388.
[38] ***National Bureau of Statistics of China, (2025), National data, retrieved November 16, 2025, from https://data.stats.gov.cn/easyquery.htm?cn=C01.